Measurement of jet suppression in central Pb–Pb collisions at $\sqrt{s_{NN}} = 2.76$ TeV

ALICE Collaboration[⋆]

A B S T R A C T

The transverse momentum (p_T) spectrum and nuclear modification factor (R_{AA}) of reconstructed jets in 0–10% and 10–30% central Pb–Pb collisions at $\sqrt{s_{NN}} = 2.76$ TeV were measured. Jets were reconstructed using the anti-k_T jet algorithm with a resolution parameter of $R = 0.2$ from charged and neutral particles, utilizing the ALICE tracking detectors and Electromagnetic Calorimeter (EMCal). The jet p_T spectra are reported in the pseudorapidity interval of $|\eta_{jet}| < 0.5$ for $40 < p_{T,\,jet} < 120$ GeV/c in 0–10% and for $30 < p_{T,\,jet} < 100$ GeV/c in 10–30% collisions. Reconstructed jets were required to contain a leading charged particle with $p_T > 5$ GeV/c to suppress jets constructed from the combinatorial background in Pb–Pb collisions. The leading charged particle requirement applied to jet spectra both in pp and Pb–Pb collisions had a negligible effect on the R_{AA}. The nuclear modification factor R_{AA} was found to be 0.28 ± 0.04 in 0–10% and 0.35 ± 0.04 in 10–30% collisions, independent of $p_{T,\,jet}$ within the uncertainties of the measurement. The observed suppression is in fair agreement with expectations from two model calculations with different approaches to jet quenching.

1. Introduction

Discrete formulations of Quantum Chromodynamics (QCD) predict the existence of a cross-over transition from normal nuclear matter to a new state of matter called the Quark–Gluon Plasma (QGP), where the partonic constituents, quarks and gluons, are deconfined. The QGP state is expected to exist at energy densities above 0.5 GeV/fm³ and temperatures above 160 MeV [1], which can be reached in collisions of heavy-ions at ultra-relativistic energies. The existence of the QGP is supported by the observations reported by experiments at the Relativistic Heavy Ion Collider (RHIC) [2–5] and at the Large Hadron Collider (LHC) [6–17].

One way to characterize the properties of the QGP is to use partons from the hard scattering of the partonic constituents in the colliding nucleons as medium probes. Hard scattering is expected to occur early in the collision evolution, producing high transverse momentum (p_T) partons, which propagate through the expanding medium and eventually fragment into jets of hadrons.

Due to interactions of the high-p_T partons with the medium, the energy of the partons is reduced compared to proton–proton (pp) collisions due to medium-induced gluon radiation and collisional energy loss (jet quenching) [18,19]. The production cross section of the initial hard scattered partons is calculable using perturbative QCD (pQCD), and the contribution from the non-perturbative hadronization can be well calibrated via jet measurements in pp collisions.

Jet quenching has been observed at RHIC [20–29] and at the LHC [8,16,17,30–41] via the measurement of inclusive hadron and jet production at high p_T, di-hadron angular correlations and the dijet energy imbalance. In all cases, the measured observable is found to be strongly modified in central heavy-ion collisions relative to pp collisions, when compared to expectations based on treating heavy-ion collisions as an incoherent superposition of independent nucleon–nucleon collisions.

Measurements of the jet kinematics are expected to be more closely correlated to the initial parton kinematics than measurements of high-p_T hadrons. Jets are usually reconstructed by grouping measured particles within a given distance, e.g. a cone with radius R. The interaction with the medium can result in a broadening of the jet shape, a softening of the jet fragmentation [42] leading to an increase of out-of-cone gluon radiation [43] with respect to jets reconstructed in pp collisions [17]. Therefore, for a given jet resolution parameter R and a fixed initial parton energy, the energy of jets reconstructed in heavy-ion collisions is expected to be smaller than those reconstructed in pp collisions.

Jet measurements in heavy-ion collisions are challenging since a single event can have multiple, possibly overlapping, jets from independent nucleon–nucleon scatters, as well as combinatoric "jets" from the large, partially correlated and fluctuating background of

⋆ *E-mail address:* alice-publications@cern.ch.

low transverse momentum particles. Consequently, jet reconstruction in heavy-ion collisions requires a robust jet-signal definition, and a procedure to correct for the presence of the large background and its associated region-to-region fluctuations [44].

The results reported in this letter are from lead–lead (Pb–Pb) collision data at an energy per nucleon pair of $\sqrt{s_{NN}} = 2.76$ TeV recorded by the ALICE detector in 2011. Charged particles are reconstructed with the Inner Tracking System (ITS) and the Time Projection Chamber (TPC) down to p_T of 0.15 GeV/c. Neutral particles, excluding neutrons and K_L^0s, are reconstructed with the Electromagnetic Calorimeter (EMCal) down to a transverse energy of the EMCal clusters of 0.3 GeV. For jet reconstruction, we followed the approach applied in Refs. [45,46], where the average energy density of the event was subtracted from the signal jets on a jet-by-jet basis, and the detector and background effects were corrected on an ensemble basis via an unfolding procedure. The signal jets were obtained using the anti-k_T jet algorithm [47] with a resolution parameter of $R = 0.2$ in the pseudorapidity range of $|\eta_{jet}| < 0.5$. Signal jets were required to contain at least one charged particle with $p_T > 5$ GeV/c. The corrected jet p_T spectra and nuclear modification factors (R_{AA}) are reported for $40 < p_{T, jet} < 120$ GeV/c in 0–10% and for $30 < p_{T, jet} < 100$ GeV/c in 10–30% central Pb–Pb collisions and the corrected jet p_T spectrum for $20 < p_{T, jet} < 120$ GeV/c in pp collisions at $\sqrt{s} = 2.76$ TeV from 13.6 nb^{-1} recorded in 2011. The R_{AA} is compared to expectations from two jet quenching model calculations with different approaches, described later, in order to test the sensitivity of the observable to the energy density via the centrality dependence, and to the parton energy scale via the momentum dependence.

2. Experimental setup

For a complete description of the ALICE detector and its performance see Refs. [48] and [49], respectively. The analysis presented here relies mainly on the ALICE tracking system and EMCal, both of which are located inside a large solenoidal magnet with field strength 0.5 T.

The tracking system consists of the ITS, a high-precision six-layer silicon detector system with the inner layer at 3.9 cm and the outer at 43 cm from the center of the detector, and the TPC with a radial extent of 85–247 cm, provides up to 159 independent space points per track. The two innermost layers of the ITS consist of the Silicon Pixel Detector (SPD), which provides two layers of silicon pixel sensors at radii 3.9 cm and 7.6 cm from the beam axis and covers the full azimuth over $|\eta| < 2$ and $|\eta| < 1.4$, respectively. The combined information of the ITS and TPC can determine the momenta of charged particles from low momentum ($p_T \approx 0.15$ GeV/c) to high momentum ($p_T \approx 100$ GeV/c) in $|\eta| < 0.9$ and full azimuth.

The EMCal is a Pb-scintillator sampling calorimeter, which covers 107 degrees in azimuth and $|\eta| < 0.7$. It consists of 10 supermodules with a total of 11 520 individual towers each covering an angular region $\Delta\eta \times \Delta\varphi = 0.014 \times 0.014$ which are read out by avalanche photodiodes.

The data were recorded in 2011 for Pb–Pb collisions at $\sqrt{s_{NN}} = 2.76$ TeV using a set of triggers based on the hit multiplicity recorded by the VZERO detector, which consists of segmented scintillators covering the full azimuth over $2.8 < \eta < 5.1$ (VZERO-A) and $-3.7 < \eta < -1.7$ (VZERO-C).

3. Data analysis

A total of 11.5M (15 μb^{-1}) and 5.7M (3.7 μb^{-1}) events with VZERO multiplicities corresponding to 0–10% and 10–30% most central events were selected using the centrality determination as

described in Ref. [50]. The accepted events, reconstructed as described in Ref. [51], were required to have a primary reconstructed vertex within 10 cm of the center of the detector.

Reconstructed tracks were required to have at least 3 hits in the ITS used in the fit to ensure adequate track momentum resolution for jet reconstruction. For tracks without any hit in the SPD, the primary vertex location was used in addition to the TPC and ITS hits for the momentum determination of the track. This reduced the azimuthal dependence of the track reconstruction efficiency due to the non-uniform SPD response, without creating track collections with drastically differing momentum resolutions. Accepted tracks were required to be measured with $0.15 < p_T < 100$ GeV/c in $|\eta| < 0.9$, and to have at least 70 TPC space-points and no less than 80% of the geometrically findable space-points in the TPC. The tracking efficiency was estimated from simulations of the detector response using GEANT3 [52] with the HIJING [53] event generator as input. In 0–10% collisions, it is about 56% at 0.15 GeV/c, about 83% at 1.5 GeV/c and then decreases to 81% at 3 GeV/c, after which it increases and levels off to about 83% at above 6.5 GeV/c. In 10–30% collisions, the tracking efficiency follows a similar p_T dependence pattern, with absolute values of the efficiency that are 1 to 2% higher compared to 0–10% collisions. The momentum resolution $\delta p_T/p_T$, estimated on a track-by-track basis using the covariance matrix of the track fit, is about 1% at 1.0 GeV/c and about 3% at 50 GeV/c. Tracks with $p_T > 50$ GeV/c were only a small contribution to the inclusive jet population considered in this analysis, for example only 20% of the jets with $p_{T, jet}$ larger than 100 GeV/c were found to contain a track above 50 GeV/c.

EMCal cells with a calibrated response of more than 50 MeV were clustered prior to inclusion in the jet finder by a clustering algorithm which required each cluster to only have a single local maximum [49]. Interactions of slow neutrons or highly ionizing particles in the avalanche photodiodes create clusters with large apparent energy, but anomalously small number of contributing cells, and are removed from the analysis. A non-linearity correction, derived from electron test beam data, of about 7% at 0.5 GeV and negligible above 3 GeV, was applied to the clusters' energies. The energy resolution obtained from electron test beam data is about 15% at 0.5 GeV and better than 5% above 3 GeV.

Unlike electrons and photons, which deposit their full energy in the EMCal via electromagnetic showering, charged hadrons deposit energy in the EMCal, mostly via minimum ionization, but also via nuclear interactions which generate hadronic showers. To avoid double counting, the energy deposited in the EMCal by charged particles that were already reconstructed as tracks, the clusters' energies were corrected by the following procedure [54]: All tracks with $p_T > 0.15$ GeV/c were propagated to the average cluster depth within the EMCal, and then associated to clusters with $E_T > 0.15$ GeV within the window $|\Delta\eta| < 0.015$ and $|\Delta\varphi| < 0.025$. Tracks were always matched to their nearest cluster, while clusters were allowed to have multiple track matches. Clusters with matched tracks were corrected for charged particle contamination by removing the fraction $f = 100\%$ of the sum of the momenta of all matched tracks from the cluster energy, as done in [54]. Clusters with $E_T > 0.30$ GeV after this correction were used in this analysis.

The collection of tracks and corrected EMCal clusters was then assembled into jets using the anti-k_T or the k_T algorithms in the FastJet package [55] with a resolution parameter of $R = 0.2$. Only those jets that were at least R away from the EMCal boundaries of $|\eta| < 0.7$ and $1.4 < \phi < \pi$, and thus fully contained within the EMCal acceptance, were kept in the analysis which limits the effect of the acceptance boundaries on the measured jet spectrum. Jets reconstructed by the anti-k_T algorithm were used to quantify

signal jets, while jets reconstructed by the k_T algorithm were used to quantify the contribution from the underlying event.

The signal spectrum formed from the reconstructed jets is affected by the contribution from the underlying event. In order to suppress the contribution of the background to the measurement of the jet energy, we followed the approach described in Refs. [45,46], which addresses the average additive contribution to the jet momentum on a jet-by-jet basis. The underlying background momentum density was estimated event-by-event using the median of $p_{T,\,jet}^{raw}/A_{jet}$, where $p_{T,\,jet}^{raw}$ is the uncorrected energy and A_{jet} is the area of jets reconstructed with the k_T algorithm. Due to the limited acceptance of the EMCal, ρ_{ch}, the median of the event-by-event momentum density distribution obtained from charged jets (i.e. jets reconstructed from tracks only) in $\left|\eta_{jet}\right| < 0.5$ and full azimuthal acceptance was used. Then, ρ_{scaled} was determined by scaling ρ_{ch} using a centrality-dependent factor. This factor is obtained from a parametrization of the measurement of the charged-to-neutral energy ratio, using tracks and corrected clusters in the EMCal acceptance. In 0–10% central Pb–Pb collisions, the average charged background momentum density was $\langle\rho_{ch}\rangle \approx 110$ GeV/c. After scaling to include the neutral component we obtained $\langle\rho_{scaled}\rangle \approx 190$ GeV/c, which corresponds to an average contribution of the underlying event of about 24 GeV/c in a cone of $R = 0.2$. In 10–30% central Pb–Pb collisions $\langle\rho_{scaled}\rangle$ decreases to ≈ 130 GeV/c. For every signal jet reconstructed with the anti-k_T algorithm, the background density scaled by the area of the reconstructed signal jet was subtracted from the reconstructed transverse momentum of the signal jet according to $p_{T,\,jet}^{reco} = p_{T,\,jet}^{raw} - \rho_{scaled} \cdot A_{jet}$.

Region-to-region background fluctuations lead to a smearing of the reconstructed jet energy. Their magnitude was estimated as described in Refs. [45,46] in two different ways: (1) by taking the scalar sum of the p_T of all particles found in a cone randomly placed in the event, referred to as random-cone method, and (2) embedding a single particle in the event and inspecting the anti-k_T jet that contains that embedded particle, referred to as embedded track method. The first method does not rely on any assumptions about the structure of the background itself and gives approximately the same background fluctuation as embedding a track with infinite momentum for anti-k_T jets. The second method should be able to reproduce the background as seen by the anti-k_T algorithm more directly. The background fluctuations were quantified by $\delta p_T = p_T^{cone} - \rho_{scaled} \cdot \pi R^2$ for the random-cone method, and $\delta p_T = p_{T,\,jet}^{reco} - p_T^{probe}$ for the embedded-track method with a minimum of $p_T^{probe} = 10$ GeV/c for the p_T of the embedded track. Above 10 GeV/c the resulting δp_T distribution does not depend on the p_T of the embedded particle. The δp_T distributions for the two methods in the 10% most central collisions are shown in Fig. 1 for $p_T^{probe} = 60$ GeV/c. The two methods appear to provide the same quantitative response to the background fluctuations, with only marginal differences mainly due to small jet area fluctuations in the embedding track method. The widths of the δp_T distributions are about 6 GeV/c. The left-hand side (LHS) of the distribution is Gaussian-like and is dominated by soft particle production. To determine its width, the distributions were fitted recursively with a Gaussian function in the range $[\mu^{LHS} - 3\sigma^{LHS}, \mu^{LHS} + \frac{1}{2}\sigma^{LHS}]$ using the mean and width of the δp_T distribution as starting values for σ and μ. The LHS width is about 5 GeV/c in 0–10% and about 3.5 GeV/c in 10–30% events. The right-hand side has additional contributions from hard scattering processes, and the resulting non-Gaussian tail at high δp_T is due to overlapping jets. The random-cone method was used as the baseline in this analysis for creating the response matrix used in unfolding, while the single
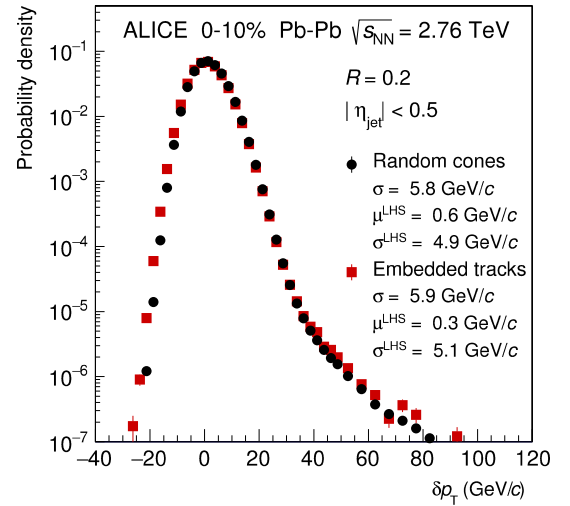

Fig. 1. The δp_T distribution for $R = 0.2$ with the random-cone and the embedded-track methods in the 10% most central events, with $p_T^{probe} = 60$ GeV/c for the embedded-track method.

particle embedding method was used to study the sensitivity of the results to the method.

Additionally, signal jets were required to contain a charged track with a transverse momentum of at least 5 GeV/c and a minimum background subtracted $p_{T,\,jet}^{reco}$ of 30 GeV/c for 0–10% and of 20 GeV/c for 10–30% most central events, which roughly corresponds to 5σ of the δp_T distribution, in order to suppress the contribution of combinatorial jets, i.e. from jets reconstructed mainly from upward fluctuations of the soft-particle background.

Both the average background and the background fluctuations are averaged over all possible orientations of the event plane, namely it is assumed that the signal jet sample being analyzed is isotropically distributed with respect to the event plane. However, the jet sample may show some degree of correlation with the event plane, both for physical reasons (e.g. path length dependence of jet energy loss) or as a result of the cuts applied in the analysis (most notably the requirement on the leading hadron p_T). Since the background is also correlated with the event plane due to flow (v_2) [10], a question may arise about the validity of this approach. Upper limits on the magnitude of these effects have been estimated by using random cones biased towards the event plane, either by requiring the presence of a 5 GeV/c track or by weighting the distribution using an upper limit on the jet v_2 of 0.1. In both cases, the upper limits on the shift of the jet energy scale (JES) were found to be smaller than 0.1 GeV/c.

4. Unfolding

The measured jet spectra are distorted by the response of the detectors used in the measurement and the background fluctuations in the underlying event. To correct for these effects we used an "unfolding" procedure, as described in Ref. [46]. The corrected distribution $p_{T,\,jet}^{true}$ and the measured distribution $p_{T,\,jet}^{reco}$ are related by a convolution through the response matrix $RM_{tot} = RM_{bkg} \times RM_{det}$, where RM_{det} parametrizes the detector response and RM_{bkg} the background fluctuations. The unfolding procedure operates under the assumption that $p_{T,\,jet}^{reco} = RM_{tot} \times p_{T,\,jet}^{true}$. Both background fluctuations and the detector response to jets are uniform within the η and φ acceptances, which is a precondition for the factorized approach used in building RM_{tot}.

The detector response for jet reconstruction was obtained using pp events simulated with the PYTHIA 6 [56] event generator

(tune A [57]). Jets were reconstructed both at "generator level" and at "detector level" using the anti-k_T algorithm. Generator-level simulations utilized only prompt particles originating from the collision (with $c\tau < 1$ cm), directly from the event generator output, without accounting for detector effects; detector-level simulations also included a detailed particle transport and detector response simulation based on GEANT3 [52] with the detector response set to the Pb–Pb configuration. During detector-level jet reconstruction, an additional p_T-dependent tracking inefficiency was introduced in order to account for the larger inefficiency due to the larger occupancy effects in central Pb–Pb events compared to pp events. Occupancy effects have been estimated comparing the tracking performance in PYTHIA and HIJING simulations, which represent pp and Pb–Pb events [53]. The occupancy effects in central HIJING events are larger for $p_T < 0.5$ GeV/c where the efficiency is about 4% lower compared to PYTHIA, and then levels off to about 2% lower for $p_T > 2$ GeV/c. In semi-central HIJING events, occupancy effects on the tracking efficiency amount to no more than 2% at low p_T and about 1% for $p_T > 2$ GeV/c. Other than this tracking efficiency correction, the detector response to jets was assumed to be the same in Pb–Pb events as in the PYTHIA simulated pp collisions.

The generator-level and detector-level jets were matched based on the Euclidean distance between their jet axes in pseudorapidity and azimuthal angle. It was ensured that the matching operation is bijective: each generator-level jet was matched to at most one detector-level jet [46]. Every matched jet pair corresponds to an entry in the detector response matrix, RM_{det}. An unmatched generator-level jet represents a jet that was not reconstructed, and this distribution was used to determine the jet reconstruction efficiency. In 0–10% Pb–Pb events, the detector jet reconstruction efficiency was found to be 90% at 40 GeV/c and 95% above 70 GeV/c, limited mainly by the track reconstruction efficiency of the leading charged particle. As described above, at detector level the constituent cut was 150 MeV/c for tracks, and 300 MeV for clusters after the cluster energy is corrected for charged particle energy contamination. However, at generator level no such cut is applied, and hence the reconstructed jets are corrected to a constituent charged particle momentum of 0 MeV/c and to a constituent cluster energy of 0 MeV in the unfolding process. A net negative shift of the JES at detector level was obtained, which originates mainly from tracking inefficiency and unreconstructed particles, such as neutrons and K_L^0, though the subtraction procedure for energy deposits by charged particles in the EMCal and missing secondary particles from weak decays contribute to the shift [54]. The JES correction applied through the response matrix is about 23% at $p_{T,jet}^{true}$ of 40 GeV/c and 29% at 120 GeV/c independent of centrality.

The RM_{bkg} matrix was constructed row-by-row by taking the δp_T distribution and shifting it along the $p_{T,jet}^{reco}$ axis by the amount $p_{T,jet}^{true}$ corresponding to each row (Toeplitz matrix). This matrix construction method assumes that the response of the jet spectrum to background fluctuations is independent of the jet momentum.

The p_T-dependence of the jet momentum resolution $\sigma(p_{T,jet}^{reco})/p_{T,jet}^{true}$ is different for the background and detector contributions [46]. The contribution from background fluctuations is dominant at low $p_{T,jet}^{true}$ and is proportional to $1/p_{T,jet}^{true}$, whereas the contribution from detector effects is fairly constant with $p_{T,jet}^{true}$. The crossover between the two contributions happens at $p_{T,jet}^{true} \approx 30$ GeV/c. The combined jet momentum resolution is about 23% at $p_{T,jet}^{true}$ of 40 GeV/c and 20% at 120 GeV/c for 0–10% collisions, while it is 24% at $p_{T,jet}^{true}$ of 30 GeV/c and 20% at 100 GeV/c for 10–30%.

Two unfolding algorithms with different regularization procedures were used for correcting the measured jet spectrum: the χ^2 minimization method [58] with a log–log-regularization and the generalized Singular Value Decomposition (SVD) method [59], as implemented in RooUnfold [60], which was used for the default value of the data points. The measured spectrum used as an input to the unfolding was in the range $30 < p_{T,jet} < 120$ GeV/c for 0–10% and $20 < p_{T,jet} < 100$ GeV/c for 10–30% collisions. A smoothed version of the measured spectrum was used as the prior, so that the statistical fluctuations within the data were not magnified in the unfolding process. The regularization parameter used for SVD unfolding is $k = 5$. The value of k is chosen such that it corresponds to the d vector magnitude of 1, and Pearson coefficients which do not show a large variation in the correlation between neighboring p_T bins.

The corrected jet spectra are reported for $40 < p_{T,jet} < 120$ GeV/c in 0–10%, and for $30 < p_{T,jet} < 100$ GeV/c in 10–30% where the efficiency due to these kinematic cuts is high, approximately 90%. It was verified that the cut on the reconstructed jet p_T has a negligible effect in the reported p_T region of the final result, as long as the requirement on the leading charged track p_T is at least 5 GeV/c. If this threshold is reduced, the cut on the minimum reconstructed jet p_T becomes crucial for unfolding stability.

The analysis procedures in the 10% most central collisions were tested with two different Monte Carlo (MC) models, where events were constructed by embedding jets into a soft background. The first test verified the robustness of the unfolding framework with the inclusion of fake "jets" that are clustered from the soft background, which did not originate from a hard process. The second model tested the assumption that the background and detector responses can be factorized.

In the first model, the soft background of both charged and neutral particles was modeled with $3100 < N_{tracks} < 5150$ where the particle transverse momenta were taken from a Boltzmann distribution with a temperature of 550 MeV. This model created a fluctuating background similar to that of the 0–10% Pb–Pb data; e.g. the background fluctuations, as estimated via the δp_T distributions, coincide within few percent. Jets were reconstructed at generator level in PYTHIA-only events and at detector level, with the added background. The first model validated the background subtraction technique, and in particular the stability of the unfolding method against the contribution from the residual combinatorial background. In the second model, the background was taken from real 0–10% Pb–Pb events. The charged particle correction for the EMCal clusters was applied after embedding. Only jets with at least 1 GeV/c of transverse momentum coming from the embedded PYTHIA event were selected for the test. This is needed to reject the signal from hard scatterings in the data, but also removes most of the combinatorial jets from the Pb–Pb underlying event. The second model was used to test the validity of the charged particle correction applied to the EMCal clusters, in particular in the interplay between the underlying event and the jets. It also validates certain aspects of the corrections applied for the background fluctuations, e.g. the unsmearing of the jet p_T due to background fluctuations or the overlap with low momentum jets. Background tracks and clusters could be matched to jet tracks and clusters or vice versa, so that the correction for charged particle contamination could potentially cause an over-subtraction that is not corrected for in the unfolding procedure. These Monte Carlo tests showed that the analysis procedures outlined above, including unfolding, recovered the input spectrum within the statistical and systematic uncertainties of the models.
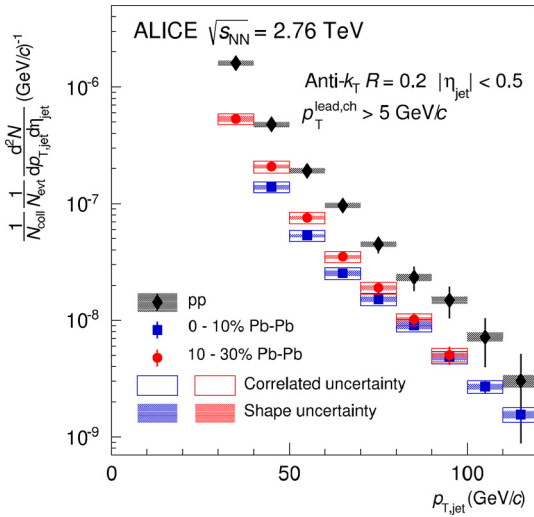
Fig. 2. The spectra of $R = 0.2$ jets with a leading track requirement of 5 GeV/c in 0–10% and 10–30% most central Pb–Pb collisions scaled by $1/N_{coll}$ and in inelastic pp collisions at $\sqrt{s_{NN}} = 2.76$ TeV. The uncertainties on the normalization are about 11% for the Pb–Pb data from the uncertainty on N_{coll} and about 8% for the pp data from the total inelastic cross section.

Table 1

Summary of systematic uncertainties for 0–10% most central collisions. The first column is the uncertainty at the minimum $p_{T, jet}^{min}$ of 40 GeV/c, the second column is the uncertainty at the maximum $p_{T, jet}^{max}$ of 120 GeV/c. The minimum and maximum columns give the extreme, and the last column gives the average systematic uncertainty over the entire p_T range. The total correlated uncertainty was calculated by adding the components in quadrature, while the shape uncertainty was calculated as the σ of the different variations (see text for details).

Category	Relative uncertainty (%)				
	$p_{T, jet}^{min}$	$p_{T, jet}^{max}$	Min.	Max.	Avg.
Tracking efficiency	7.7	11.3	7.3	11.3	8.8
Track momentum resolution	1.0	1.0	1.0	1.0	1.0
Charged particle correction	0.7	2.7	0.7	6.4	3.7
EMCal clusterizer	3.2	1.8	0.1	3.2	1.4
EMCal response	4.4	4.4	4.4	4.4	4.4
Background fluctuations	3.9	2.7	2.3	3.9	2.8
Jet raw p_T cuts	2.6	6.7	1.5	6.7	3.6
Combinatorial jets	0.3	0.5	0.0	0.5	0.2
Total correlated uncertainty	10.6	14.5	10.6	14.5	12.0
Unfolding method	0.1	10.0	0.1	15.5	6.6
SVD reg. param. $k = 4$	3.6	11.7	2.4	11.7	6.0
SVD reg. param. $k = 6$	7.2	2.7	1.5	8.8	5.3
Prior choice 1	1.9	4.0	0.2	4.0	1.6
Prior choice 2	2.1	1.4	0.1	2.1	0.9
Total shape uncertainty	3.8	7.2	2.7	7.4	5.3

5. Results

The unfolded jet spectra in 0–10% and 10–30% central collisions are displayed in Fig. 2. To compare the spectra with the spectrum measured in pp collisions, the yield is divided by the number of binary collisions, which is $N_{coll} = 1501 \pm 167$ for 0–10% and 743 ± 79 for 10–30% collisions, as estimated from a Glauber MC calculation [50].

The systematic uncertainties on the jet spectrum are summarized in Table 1 for the 0–10% centrality class. For the 10–30% centrality class the corresponding uncertainties differ, on average, by 2% or less. The systematic uncertainties were divided into two categories: correlated uncertainties and shape uncertainties. The correlated uncertainties result dominantly from uncertainties on the JES, such as the uncertainty of the tracking efficiency, that will shift the entire jet spectrum in one direction, whereas the shape

uncertainties are related to the unfolding and can distort the slope of the spectrum.

The dominant correlated uncertainty on the jet spectrum of about 9% arises from the uncertainty on the tracking efficiency. It is estimated by varying the tracking efficiency by 5% in determining RM_{det} and unfolding the spectrum. The uncertainty due to the correction procedure for the charged particle double counting in the EMCal of about 4% was determined by varying f from 100% to 30% in both the measured spectrum and the RM_{det}. The determination of the uncertainties from other EMCal response related uncertainties as EMCal energy scale, EMCal energy resolution, and EMCal non-linearity is outlined in [54] and combined leads to an uncertainty of 4.4%. The uncertainty arising from the choice of the EMCal clustering algorithm is determined by using a different clusterizing method, that forms fixed-size clusters from 3×3 towers. For the background fluctuations, the response matrix RM_{bkg} was constructed with the single-track embedding method for determining δp_T, as discussed above. To estimate the sensitivity of the unfolding to the raw jet p_T selection, the p_T range of input spectra is varied by extending the range at both the low and high ends by ± 5 GeV/c. The influence of combinatorial jets, estimated by varying the low edge of the unfolded spectrum from 0 to up to 10 GeV/c was found to be negligible. Since all sources of uncertainty are independent, each contribution is added in quadrature to obtain the final correlated uncertainty of 10.6% to 14.5% as listed in Table 1. The uncertainty on the JES is 2.4% to 3.2% and can be obtained by dividing the uncertainties listed in Table 1 by 4.5, where the exponent $n = 4.5$ was obtained by fitting a power law to the measured spectrum.

The shape uncertainty is dominated by the regularization used in the unfolding and can be divided into two components: the method by which the solution is regularized, e.g. χ^2 instead of the SVD unfolding, and the variation of the regularization process within a given method. The regularization is done by adding a penalty term in the χ^2 method and by ignoring the components of the SVD decomposition that are dominated by statistical fluctuations. For the SVD method, the regularization k factor is an integer value and thus can only be varied in integer steps. The uncertainty related to the choice of the prior is estimated by varying the exponent of the power law function extracted from the reconstructed spectrum by ± 0.5, which is used to construct the prior. The uncertainty related to the choice of the prior is estimated by varying the exponent $n = 4.5$ by ± 0.5 to scale the prior. The differences in the unfolded spectrum with these variations are summarized in Table 1. These variations in the regularization strategy are combined assuming that they constitute independent measurements. The final shape uncertainty is thus obtained by summing them in quadrature and dividing by the square root of the number of variations.

The jet spectrum in pp collisions was measured in the same way as reported in Ref. [54], but with the 5 GeV/c leading charged particle requirement necessary for the Pb–Pb analysis. The resulting spectrum normalized per inelastic pp collision is shown in Fig. 2. In order to determine the effect of the leading track requirement in pp collisions, the ratio of the jet spectra with a 5 GeV/c leading track requirement (the biased jet sample), over the spectrum of jets without a leading track requirement (the inclusive jet sample) with resolution parameter $R = 0.2$ is shown in Fig. 3. Systematic uncertainties in the ratio were evaluated by removing the uncertainties that are correlated between the spectra obtained with and without the cut on the leading particle. As can be seen in Fig. 3, for $p_{T, jet}$ above 50 GeV/c more than 95% of all reconstructed jets have at least one track with a p_T greater than 5 GeV/c. PYTHIA tune A (but also other common tunes like the Perugia tunes [57]) accurately describes the measured ratio.
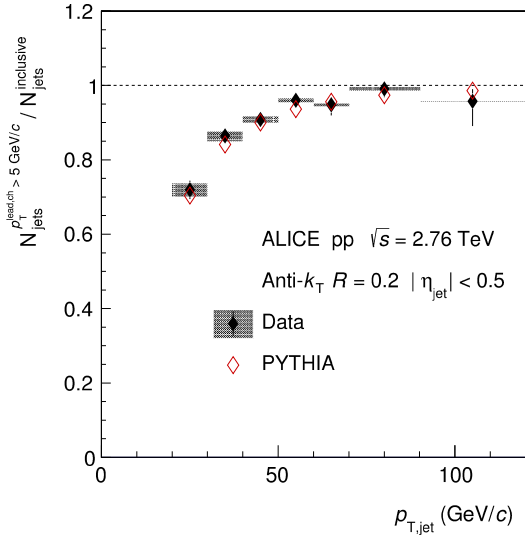
Fig. 3. Ratio of the jet spectrum with a leading track $p_T > 5$ GeV/c over the inclusive jet spectrum for $R = 0.2$ in pp collisions at $\sqrt{s} = 2.76$ TeV.

The influence of the leading track requirement in the Pb–Pb measurement, nominally set to 5 GeV/c was tested by varying it by 40%, i.e. reducing it to 3 and increasing it to 7 GeV/c, and with the more extreme values of 0 and 10 GeV/c. The ratios of jet spectra with the different leading track p_T biases, after all corrections, are shown in Fig. 4 for $R = 0.2$ jets in 0–10% central Pb–Pb collisions at $\sqrt{s_{NN}} = 2.76$ TeV. The corrections to these different jet spectra were done using the same unfolding procedure as the nominal spectrum with leading track p_T bias of 5 GeV/c, with a slightly modified response matrix which accounts for the different biases. Since the unfolding procedure weakens the correlation between the statistical fluctuations of the jet spectra with different leading track requirements, the statistical uncertainties have been added in quadrature in the ratio. The systematic shape uncertainty is due to the unfolding procedure, and has been treated as completely uncorrelated in the ratio. The correlated uncertainty is primarily due to the uncertainty on the JES, which is highly correlated between the various spectra. The systematic variations in the unfolding procedure have been applied consistently for both the denominator (with a leading track $p_T > 5$ GeV/c) and the numerators (with a 0, 3, 7 and 10 GeV/c leading track bias), and the resulting difference in the ratios has been taken as a systematic uncertainty. The jet spectra with leading track requirements of 3 and 0 GeV/c are consistent with the baseline measurement

with a 5 GeV/c requirement. The unfolding is not as stable as with a 5 GeV/c requirement, which leads to a larger systematic uncertainty due to the unfolding correction procedure, especially for the inclusive spectrum. All measurements of the ratio of jet spectra with different leading track biases, particularly those with a higher leading track p_T requirement than the nominal, are well described by PYTHIA 6 (tune A), within one sigma of the uncertainties or less.

The nuclear modification factor, R_{AA}, is defined as the ratio of the jet spectrum in Pb–Pb divided by the spectrum in pp collisions scaled by N_{coll}. It is constructed such that R_{AA} equals unity if there is no net nuclear modification of the spectrum in Pb–Pb collisions as compared to an incoherent superposition of independent pp collisions. The resulting R_{AA} of jets with a 5 GeV/c leading track requirement for $R = 0.2$ in the 0–10% and 10–30% central Pb–Pb collisions is reported in Fig. 5. The systematic and statistical uncertainties from the Pb–Pb and pp measurements (see Fig. 2) are added in quadrature. The resulting uncertainty on the normalization is from scaling the pp cross section with the nuclear overlap $T_{AA} = 23.5 \pm 0.87$ mb^{-1} for 0–10% and 11.6 ± 0.60 mb^{-1} for 10–30% collisions. As can be seen, jets in the measured $p_{T, jet}$ range are strongly suppressed. The average R_{AA} in both 0–10% and 10–30% central events was found to have a negligible $p_{T, jet}$ dependence. In the 10% most central events, combining the statistical and systematic uncertainty in quadrature, the average R_{AA} is found to be 0.28 ± 0.04. The suppression is smaller in magnitude in the 10–30% central events, leading to an average R_{AA} of 0.35 ± 0.04. These results qualitatively agree with the suppression obtained from measurements using charged-particle jets [46], though the jet energy scale is not the same in both cases, and so a direct comparison is not possible. Furthermore, the results are consistent with the R_{AA} reported by ATLAS for $R = 0.4$ jets scaled by the ratio of the yields with the different resolution parameters in different $p_{T, jet}$ bins [36,41].

In order to interpret the results and move to a more quantitative understanding of jet quenching mechanisms, a comparison of the measured R_{AA} in 0–10% central collisions to calculations from two different models is also shown in Fig. 5. The first model, Ya-JEM [61], uses a $2 + 1$D hydrodynamical calculation and a Glauber MC for the initial geometry, as well as a LO pQCD calculation to determine the outgoing partons. Parton showers are modified by a medium-induced increase of the virtuality during their evolution through the medium. The Lund model in PYTHIA is used for hadronization into final state particles. The kinematics of the virtual partons in the evolving partonic shower were modified with a parameter related to the two transport coefficients, $\hat{q}$ and $\hat{e}$, that describes how strongly a parton of a given momentum couples to
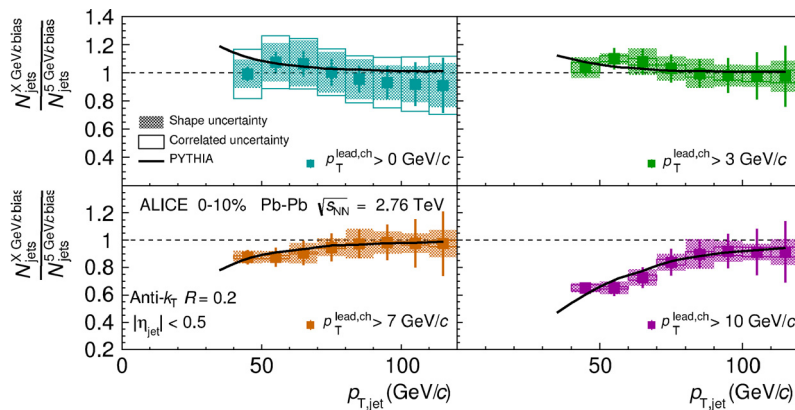

Fig. 4. Ratios of jet spectra with different leading track p_T requirements ("0 over 5", "3 over 5", "7 over 5" and "10 over 5") for $R = 0.2$ jets in 0–10% Pb–Pb collisions at $\sqrt{s_{NN}} = 2.76$ TeV. The solid black lines represent predictions from PYTHIA.
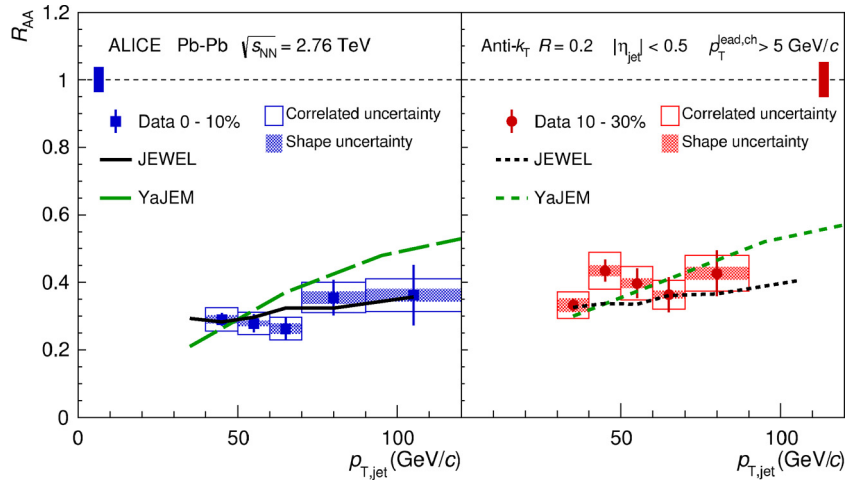
Fig. 5. R_{AA} for $R = 0.2$ jets with the leading track requirement of 5 GeV/c in 0–10% (left) and 10–30% (right) most central Pb–Pb collisions compared to calculations from YaJEM [61] and JEWEL [62]. The boxes at $R_{AA} = 1$ represent the systematic uncertainty on T_{AA}.

the medium. The parameter was fixed so that the model accurately describes the R_{AA} for charged hadrons at 10 GeV/c [17], but no additional changes were made for the prediction of the jet R_{AA}. The second model, JEWEL [62], takes a different approach in the description of the parton–medium interaction by giving a microscopical description of the transport coefficient, $\hat{q}$. Essentially each scattering of the initial parton with medium partons is computed and the average over all scatters determines $\hat{q}$. JEWEL uses a combination of Glauber and PYTHIA to determine the initial geometry, a 1D Bjorken expansion for the medium evolution, and PYTHIA for hadronization into final state particles. The transverse medium density profile in JEWEL is proportional to the density of wounded nucleons combined with a 1D Bjorken expansion for the time evolution. Hard scatters are generated according to Glauber collision geometry, and suffer from elastic and radiative energy loss in the medium, including a Monte Carlo implementation of LPM interference effects. PYTHIA is used for the hadronization of final state particles. Despite their different approaches, both calculations are found to reproduce the jet suppression. YaJEM, however, exhibits a slightly steeper increase with jet p_T than the data. The calculated χ^2 are 1.690 for YaJEM and 0.368 for JEWEL, obtained by comparing the models with the data. Additional measurements will be needed in order to further constrain the models, such as measuring the jet suppression relative to the event plane angle, which would require a more accurate modeling of the path-length dependence of jet quenching.

6. Summary

The transverse momentum (p_T) spectrum and nuclear modification factor (R_{AA}) of jets reconstructed from charged particles measured by the ALICE tracking system and neutral energy measured by the ALICE Electromagnetic Calorimeter are measured with $R = 0.2$ in the range of $40 < p_{T,\,jet} < 120$ GeV/c for 0–10% and in $30 < p_{T,\,jet} < 100$ GeV/c for 10–30% most central Pb–Pb collisions at $\sqrt{s_{NN}} = 2.76$ TeV were measured. The jets were required to contain at least one charged particle with $p_T > 5$ GeV/c. The effect of this requirement on the reported R_{AA} was evaluated by the ratios of the jet spectra with the 5 GeV/c to no requirement compared to expectations on PYTHIA, and found not to have an observable effect within the uncertainties of the measurement. Jets with $40 < p_{T,\,jet} < 120$ GeV/c are strongly suppressed in the 10% most central events, with R_{AA} about 0.28 ± 0.04, independent of $p_{T,\,jet}$ within the uncertainties of the measurement. The suppression in 10–30% events is 0.35 ± 0.04, slightly less than in the most

central events. The observed suppression is in fair agreement with expectations from two jet quenching model calculations.

References

[1] HotQCD Collaboration, T. Bhattacharya, M.I. Buchoff, N.H. Christ, et al., QCD phase transition with chiral quarks and physical quark masses, Phys. Rev. Lett. 113 (Aug 2014) 082001, arXiv:1402.5175 [hep-lat], http://link.aps.org/doi/10.1103/PhysRevLett.113.082001.

[2] BRAHMS Collaboration, I. Arsene, et al., Quark–gluon plasma and color glass condensate at RHIC? The perspective from the BRAHMS experiment, Nucl. Phys. A 757 (1–2) (2005) 1–27.

[3] PHOBOS Collaboration, B. Back, et al., The PHOBOS perspective on discoveries at RHIC, Nucl. Phys. A 757 (1–2) (2005) 28–101.

[4] PHENIX Collaboration, K. Adcox, et al., Formation of dense partonic matter in relativistic nucleus–nucleus collisions at RHIC: experimental evaluation by the PHENIX Collaboration, Nucl. Phys. A 757 (1–2) (2005) 184–283.

[5] STAR Collaboration, J. Adams, et al., Experimental and theoretical challenges in the search for the quark–gluon plasma: the STAR Collaboration's critical assessment of the evidence from RHIC collisions, Nucl. Phys. A 757 (1–2) (2005) 102–183.

[6] ALICE Collaboration, K. Aamodt, et al., Charged-particle multiplicity density at mid-rapidity in central Pb–Pb collisions at $\sqrt{s_{NN}} = 2.76$ TeV, Phys. Rev. Lett. 105 (2010) 252301, arXiv:1011.3916 [nucl-ex].

[7] ALICE Collaboration, K. Aamodt, et al., Centrality dependence of the charged-particle multiplicity density at mid-rapidity in Pb–Pb collisions at $\sqrt{s_{NN}} = 2.76$ TeV, Phys. Rev. Lett. 106 (2011) 032301, arXiv:1012.1657 [nucl-ex].

[8] CMS Collaboration, S. Chatrchyan, et al., Dependence on pseudorapidity and centrality of charged hadron production in Pb–Pb collisions at a nucleon–nucleon centre-of-mass energy of 2.76 TeV, J. High Energy Phys. 1108 (2011) 141, arXiv:1107.4800 [nucl-ex].

[9] ALICE Collaboration, K. Aamodt, et al., Two-pion Bose–Einstein correlations in central Pb–Pb collisions at $\sqrt{s_{NN}} = 2.76$ TeV, Phys. Lett. B 696 (2011) 328–337, arXiv:1012.4035 [nucl-ex].

[10] ALICE Collaboration, K. Aamodt, et al., Elliptic flow of charged particles in Pb–Pb collisions at 2.76 TeV, Phys. Rev. Lett. 105 (2010) 252302, arXiv:1011.3914 [nucl-ex].

[11] ATLAS Collaboration, G. Aad, et al., Measurement of the pseudorapidity and transverse momentum dependence of the elliptic flow of charged particles in lead–lead collisions at $\sqrt{s_{NN}} = 2.76$ TeV with the ATLAS detector, Phys. Lett. B 707 (2012) 330–348, arXiv:1108.6018 [hep-ex].

[12] CMS Collaboration, S. Chatrchyan, et al., Centrality dependence of dihadron correlations and azimuthal anisotropy harmonics in Pb–Pb collisions at $\sqrt{s_{NN}} = 2.76$ TeV, Eur. Phys. J. C 72 (2012) 2012, arXiv:1201.3158 [nucl-ex].

[13] ALICE Collaboration, K. Aamodt, et al., Higher harmonic anisotropic flow measurements of charged particles in Pb–Pb collisions at $\sqrt{s_{NN}} = 2.76$ TeV, Phys. Rev. Lett. 107 (2011) 032301, arXiv:1105.3865 [nucl-ex].

[14] ATLAS Collaboration, G. Aad, et al., Measurement of the distributions of event-by-event flow harmonics in lead–lead collisions at 2.76 TeV with the ATLAS detector at the LHC, J. High Energy Phys. 1311 (2013) 183, arXiv:1305.2942 [hep-ex].

[15] CMS Collaboration, S. Chatrchyan, et al., Measurement of higher-order harmonic azimuthal anisotropy in Pb–Pb collisions at $\sqrt{s_{NN}} = 2.76$ TeV, Phys. Rev. C 89 (2014) 044906, arXiv:1310.8651 [nucl-ex].

[16] ALICE Collaboration, K. Aamodt, et al., Suppression of charged particle production at large transverse momentum in central Pb–Pb collisions at $\sqrt{s_{NN}} = 2.76$ TeV, Phys. Lett. B 696 (2011) 30–39, arXiv:1012.1004 [nucl-ex].

[17] CMS Collaboration, S. Chatrchyan, et al., Observation and studies of jet quenching in Pb–Pb collisions at nucleon–nucleon center-of-mass energy of 2.76 TeV, Phys. Rev. C 84 (2011) 024906, arXiv:1102.1957 [nucl-ex].

[18] M. Gyulassy, M. Plumer, Jet quenching in dense matter, Phys. Lett. B 243 (1990) 432–438.

[19] R. Baier, Y.L. Dokshitzer, S. Peigne, D. Schiff, Induced gluon radiation in a QCD medium, Phys. Lett. B 345 (1995) 277–286, arXiv:hep-ph/9411409.

[20] PHENIX Collaboration, K. Adcox, et al., Suppression of hadrons with large transverse momentum in central Au + Au collisions at $\sqrt{s_{NN}} = 130$ GeV, Phys. Rev. Lett. 88 (2002) 022301, arXiv:nucl-ex/0109003.

[21] STAR Collaboration, C. Adler, et al., Disappearance of back-to-back high p_T hadron correlations in central Au + Au collisions at $\sqrt{s_{NN}} = 200$ GeV, Phys. Rev. Lett. 90 (2003) 082302, arXiv:nucl-ex/0210033.

[22] PHENIX Collaboration, K. Adcox, et al., Centrality dependence of the high-p_T charged hadron suppression in Au + Au collisions at $\sqrt{s_{NN}} = 130$ GeV, Phys. Lett. B 561 (2003) 82–92, arXiv:nucl-ex/0207009.

[23] PHENIX Collaboration, S.S. Adler, et al., Suppressed π^0 production at large transverse momentum in central Au + Au collisions at $\sqrt{s_{NN}} = 200$ GeV, Phys. Rev. Lett. 91 (2003) 072301, arXiv:nucl-ex/0304022.

[24] STAR Collaboration, J. Adams, et al., Transverse-momentum and collision-energy dependence of high-p_T hadron suppression in Au + Au collisions at ultrarelativistic energies, Phys. Rev. Lett. 91 (Oct 2003) 172302, arXiv:nucl-ex/0305015.

[25] STAR Collaboration, J. Adams, et al., Evidence from d + Au measurements for final state suppression of high-p_T hadrons in Au + Au collisions at RHIC, Phys. Rev. Lett. 91 (2003) 072304, arXiv:nucl-ex/0306024.

[26] PHOBOS Collaboration, B. Back, et al., Charged hadron transverse momentum distributions in Au + Au collisions at $\sqrt{s_{NN}} = 200$ GeV, Phys. Lett. B 578 (2004) 297–303, arXiv:nucl-ex/0302015.

[27] BRAHMS Collaboration, I. Arsene, et al., Transverse momentum spectra in Au + Au and d + Au collisions at $\sqrt{s_{NN}} = 200$ GeV and the pseudorapidity dependence of high-p_T suppression, Phys. Rev. Lett. 91 (2003) 072305, arXiv:nucl-ex/0307003.

[28] PHENIX Collaboration, A. Adare, et al., System size and energy dependence of jet-induced hadron pair correlation shapes in Cu + Cu and Au + Au collisions at $\sqrt{s_{NN}} = 200$ and 62.4 GeV, Phys. Rev. Lett. 98 (2007) 232302, arXiv:nucl-ex/0611019.

[29] PHENIX Collaboration, A. Adare, et al., Quantitative constraints on the opacity of hot partonic matter from semi-inclusive single high transverse momentum pion suppression in Au + Au collisions at $\sqrt{s_{NN}} = 200$ GeV, Phys. Rev. C 77 (2008) 064907, arXiv:0801.1665 [nucl-ex].

[30] ATLAS Collaboration, G. Aad, et al., Observation of a centrality-dependent dijet asymmetry in Pb–Pb collisions at $\sqrt{s_{NN}} = 2.76$ TeV with the ATLAS detector at the LHC, Phys. Rev. Lett. 105 (2010) 252303, arXiv:1011.6182 [hep-ex].

[31] ALICE Collaboration, K. Aamodt, et al., Particle-yield modification in jet-like azimuthal di-hadron correlations in Pb–Pb collisions at $\sqrt{s_{NN}} = 2.76$ TeV, Phys. Rev. Lett. 108 (2012) 092301, arXiv:1110.0121 [nucl-ex].

[32] CMS Collaboration, S. Chatrchyan, et al., Study of high-p_T charged particle suppression in Pb–Pb compared to pp collisions at $\sqrt{s_{NN}} = 2.76$ TeV, Eur. Phys. J. C 72 (2012) 1945, arXiv:1202.2554 [nucl-ex].

[33] CMS Collaboration, S. Chatrchyan, et al., Jet momentum dependence of jet quenching in Pb–Pb collisions at $\sqrt{s_{NN}} = 2.76$ TeV, Phys. Lett. B 712 (2012) 176–197, arXiv:1202.5022 [nucl-ex].

[34] CMS Collaboration, S. Chatrchyan, et al., Measurement of jet fragmentation into charged particles in pp and Pb–Pb collisions at $\sqrt{s_{NN}} = 2.76$ TeV, J. High Energy Phys. 1210 (2012) 087, arXiv:1205.5872 [nucl-ex].

[35] CMS Collaboration, S. Chatrchyan, et al., Studies of jet quenching using isolated-photon + jet correlations in Pb–Pb and pp collisions at $\sqrt{s_{NN}} = 2.76$ TeV, Phys. Lett. B 718 (2013) 773–794, arXiv:1205.0206 [nucl-ex].

[36] ATLAS Collaboration, G. Aad, et al., Measurement of the jet radius and transverse momentum dependence of inclusive jet suppression in lead–lead collisions at $\sqrt{s_{NN}} = 2.76$ TeV with the ATLAS detector, Phys. Lett. B 719 (2013) 220–241, arXiv:1208.1967 [hep-ex].

[37] CMS Collaboration, S. Chatrchyan, et al., Evidence of b-jet quenching in Pb–Pb collisions at $\sqrt{s_{NN}} = 2.76$ TeV, Phys. Rev. Lett. 113 (13) (2014) 132301, arXiv:1312.4198 [nucl-ex].

[38] CMS Collaboration, S. Chatrchyan, et al., Modification of jet shapes in Pb–Pb collisions at $\sqrt{s_{NN}} = 2.76$ TeV, Phys. Lett. B 730 (2014) 243–263, arXiv:1310.0878 [nucl-ex].

[39] CMS Collaboration, S. Chatrchyan, et al., Measurement of jet fragmentation in Pb–Pb and pp collisions at $\sqrt{s_{NN}} = 2.76$ TeV, arXiv:1406.0932 [nucl-ex].

[40] ATLAS Collaboration, G. Aad, et al., Measurement of inclusive jet charged-particle fragmentation functions in Pb + Pb collisions at $\sqrt{s_{NN}} = 2.76$ TeV with the ATLAS detector, arXiv:1406.2979 [hep-ex].

[41] ATLAS Collaboration, G. Aad, et al., Measurements of the nuclear modification factor for jets in Pb–Pb collisions at $\sqrt{s_{NN}} = 2.76$ TeV with the ATLAS detector, arXiv:1411.2357 [hep-ex].

[42] C.A. Salgado, U.A. Wiedemann, Medium modification of jet shapes and jet multiplicities, Phys. Rev. Lett. 93 (2004) 042301, arXiv:hep-ph/0310079.

[43] I. Vitev, Large angle hadron correlations from medium-induced gluon radiation, Phys. Lett. B 630 (2005) 78–84, arXiv:hep-ph/0501255.

[44] M. Cacciari, J. Rojo, G.P. Salam, G. Soyez, Jet reconstruction in heavy ion collisions, Eur. Phys. J. C 71 (2011) 1539, arXiv:1010.1759 [hep-ph].

[45] ALICE Collaboration, B. Abelev, et al., Measurement of event background fluctuations for charged particle jet reconstruction in Pb–Pb collisions at $\sqrt{s_{NN}} = 2.76$ TeV, J. High Energy Phys. 1203 (2012) 053, arXiv:1201.2423 [hep-ex].

[46] ALICE Collaboration, B. Abelev, et al., Measurement of charged jet suppression in Pb–Pb collisions at $\sqrt{s_{NN}} = 2.76$ TeV, J. High Energy Phys. 1403 (2014) 013, arXiv:1311.0633 [nucl-ex].

[47] M. Cacciari, G.P. Salam, G. Soyez, The anti-k(t) jet clustering algorithm, J. High Energy Phys. 0804 (2008) 063, arXiv:0802.1189 [hep-ph].

[48] ALICE Collaboration, K. Aamodt, et al., The ALICE experiment at the CERN LHC, J. Instrum. 3 (2008) S08002.

[49] ALICE Collaboration, B.B. Abelev, et al., Performance of the ALICE experiment at the CERN LHC, Int. J. Mod. Phys. A 29 (2014) 1430044, arXiv:1402.4476 [nucl-ex].

[50] ALICE Collaboration, B. Abelev, et al., Centrality determination of Pb–Pb collisions at $\sqrt{s_{NN}} = 2.76$ TeV with ALICE, Phys. Rev. C 88 (4) (2013) 044909, arXiv:1301.4361 [nucl-ex].

[51] ALICE Collaboration, B. Abelev, et al., Centrality dependence of charged particle production at large transverse momentum in Pb–Pb collisions at $\sqrt{s_{NN}} = 2.76$ TeV, Phys. Lett. B 720 (2013) 52–62, arXiv:1208.2711 [hep-ex].

[52] R. Brun, F. Carminati, S. Giani, GEANT detector description and simulation tool, CERN Program Library Long Write-up, W5013, 1994.

[53] X.-N. Wang, M. Gyulassy, HIJING: a Monte Carlo model for multiple jet production in pp, pA and AA collisions, Phys. Rev. D 44 (1991) 3501.

[54] ALICE Collaboration, B. Abelev, et al., Measurement of the inclusive differential jet cross section in pp collisions at $\sqrt{s} = 2.76$ TeV, Phys. Lett. B 722 (2013) 262–272, arXiv:1301.3475 [nucl-ex].

[55] M. Cacciari, G.P. Salam, G. Soyez, FastJet user manual, Eur. Phys. J. C 72 (2012) 1896, arXiv:1111.6097 [hep-ph].

[56] T. Sjostrand, S. Mrenna, P.Z. Skands, PYTHIA 6.4 physics and manual, J. High Energy Phys. 0605 (2006) 026, arXiv:hep-ph/0603175.

[57] P.Z. Skands, Tuning Monte Carlo generators: the Perugia tunes, Phys. Rev. D 82 (2010) 074018, arXiv:1005.3457 [hep-ph].

[58] C. Verkerk, CERN School of Computing, Aiguablava, Spain, 9–22 Sep 1984, Proceedings.

[59] A. Hocker, V. Kartvelishvili, SVD approach to data unfolding, Nucl. Instrum. Methods A 372 (1996) 469–481, arXiv:hep-ph/9509307.

[60] CERN, PHYSTAT 2011 Workshop on Statistical Issues Related to Discovery Claims in Search Experiments and Unfolding, CERN, Geneva, 2011.

[61] T. Renk, Physics probed by the P_T dependence of the nuclear suppression factor, Phys. Rev. C 88 (1) (2013) 014905, arXiv:1302.3710 [hep-ph].

[62] K.C. Zapp, F. Krauss, U.A. Wiedemann, A perturbative framework for jet quenching, J. High Energy Phys. 1303 (2013) 080, arXiv:1212.1599 [hep-ph].

ALICE Collaboration

J. Adam [39], D. Adamová [82], M.M. Aggarwal [86], G. Aglieri Rinella [36], M. Agnello [110], N. Agrawal [47], Z. Ahammed [130], I. Ahmed [16], S.U. Ahn [67], I. Aimo [93,110], S. Aiola [135], M. Ajaz [16], A. Akindinov [57], S.N. Alam [130], D. Aleksandrov [99], B. Alessandro [110], D. Alexandre [101], R. Alfaro Molina [63], A. Alici [104,12], A. Alkin [3], J. Alme [37], T. Alt [42], S. Altinpinar [18], I. Altsybeev [129], C. Alves Garcia Prado [118], C. Andrei [77], A. Andronic [96], V. Anguelov [92], J. Anielski [53], T. Antičić [97], F. Antinori [107], P. Antonioli [104], L. Aphecetche [112], H. Appelshäuser [52], S. Arcelli [28], N. Armesto [17], R. Arnaldi [110], T. Aronsson [135], I.C. Arsene [22], M. Arslandok [52], A. Augustinus [36], R. Averbeck [96], M.D. Azmi [19], M. Bach [42], A. Badalà [106], Y.W. Baek [43], S. Bagnasco [110], R. Bailhache [52], R. Bala [89], A. Baldisseri [15], M. Ball [91], F. Baltasar Dos Santos Pedrosa [36], R.C. Baral [60], A.M. Barbano [110], R. Barbera [29], F. Barile [33], G.G. Barnaföldi [134], L.S. Barnby [101], V. Barret [69], P. Bartalini [7], J. Bartke [115], E. Bartsch [52], M. Basile [28], N. Bastid [69], S. Basu [130], B. Bathen [53], G. Batigne [112], A. Batista Camejo [69], B. Batyunya [65], P.C. Batzing [22], I.G. Bearden [79], H. Beck [52], C. Bedda [110], N.K. Behera [47], I. Belikov [54], F. Bellini [28], H. Bello Martinez [2], R. Bellwied [120], R. Belmont [133], E. Belmont-Moreno [63], V. Belyaev [75], G. Bencedi [134], S. Beole [27], I. Berceanu [77], A. Bercuci [77], Y. Berdnikov [84], D. Berenyi [134], R.A. Bertens [56], D. Berzano [36,27], L. Betev [36], A. Bhasin [89], I.R. Bhat [89], A.K. Bhati [86], B. Bhattacharjee [44], J. Bhom [126], L. Bianchi [27,120], N. Bianchi [71], C. Bianchin [133,56], J. Bielčík [39], J. Bielčíková [82], A. Bilandzic [79], S. Biswas [78], S. Bjelogrlic [56], F. Blanco [10], D. Blau [99], C. Blume [52], F. Bock [73,92], A. Bogdanov [75], H. Bøggild [79], L. Boldizsár [134], M. Bombara [40], J. Book [52], H. Borel [15], A. Borissov [95], M. Borri [81], F. Bossú [64], M. Botje [80], E. Botta [27], S. Böttger [51], P. Braun-Munzinger [96], M. Bregant [118], T. Breitner [51], T.A. Broker [52], T.A. Browning [94], M. Broz [39], E.J. Brucken [45], E. Bruna [110], G.E. Bruno [33], D. Budnikov [98], H. Buesching [52], S. Bufalino [36,110], P. Buncic [36], O. Busch [92], Z. Buthelezi [64], J.T. Buxton [20], D. Caffarri [30,36], X. Cai [7], H. Caines [135], L. Calero Diaz [71], A. Caliva [56], E. Calvo Villar [102], P. Camerini [26], F. Carena [36], W. Carena [36], J. Castillo Castellanos [15], A.J. Castro [123], E.A.R. Casula [25], C. Cavicchioli [36], C. Ceballos Sanchez [9], J. Cepila [39], P. Cerello [110], B. Chang [121], S. Chapeland [36], M. Chartier [122], J.L. Charvet [15], S. Chattopadhyay [130], S. Chattopadhyay [100], V. Chelnokov [3], M. Cherney [85], C. Cheshkov [128], B. Cheynis [128], V. Chibante Barroso [36], D.D. Chinellato [119], P. Chochula [36], K. Choi [95], M. Chojnacki [79], S. Choudhury [130], P. Christakoglou [80], C.H. Christensen [79], P. Christiansen [34], T. Chujo [126], S.U. Chung [95], C. Cicalo [105], L. Cifarelli [12,28], F. Cindolo [104], J. Cleymans [88], F. Colamaria [33], D. Colella [33], A. Collu [25], M. Colocci [28], G. Conesa Balbastre [70], Z. Conesa del Valle [50], M.E. Connors [135], J.G. Contreras [11,39], T.M. Cormier [83], Y. Corrales Morales [27], I. Cortés Maldonado [2], P. Cortese [32], M.R. Cosentino [118], F. Costa [36], P. Crochet [69], R. Cruz Albino [11], E. Cuautle [62], L. Cunqueiro [36], T. Dahms [91], A. Dainese [107], A. Danu [61], D. Das [100], I. Das [100,50], S. Das [4], A. Dash [119], S. Dash [47], S. De [118],

A. De Caro [31,12], G. de Cataldo [103], J. de Cuveland [42], A. De Falco [25], D. De Gruttola [12,31], N. De Marco [110], S. De Pasquale [31], A. Deisting [96,92], A. Deloff [76], E. Dénes [134], G. D'Erasmo [33], D. Di Bari [33], A. Di Mauro [36], P. Di Nezza [71], M.A. Diaz Corchero [10], T. Dietel [88], P. Dillenseger [52], R. Divià [36], Ø. Djuvsland [18], A. Dobrin [56,80], T. Dobrowolski [76,i], D. Domenicis Gimenez [118], B. Dönigus [52], O. Dordic [22], A.K. Dubey [130], A. Dubla [56], L. Ducroux [128], P. Dupieux [69], R.J. Ehlers [135], D. Elia [103], H. Engel [51], B. Erazmus [112,36], F. Erhardt [127], D. Eschweiler [42], B. Espagnon [50], M. Estienne [112], S. Esumi [126], J. Eum [95], D. Evans [101], S. Evdokimov [111], G. Eyyubova [39], L. Fabbietti [91], D. Fabris [107], J. Faivre [70], A. Fantoni [71], M. Fasel [73], L. Feldkamp [53], D. Felea [61], A. Feliciello [110], G. Feofilov [129], J. Ferencei [82], A. Fernández Téllez [2], E.G. Ferreiro [17], A. Ferretti [27], A. Festanti [30], J. Figiel [115], M.A.S. Figueredo [122], S. Filchagin [98], D. Finogeev [55], F.M. Fionda [103], E.M. Fiore [33], M. Floris [36], S. Foertsch [64], P. Foka [96], S. Fokin [99], E. Fragiacomo [109], A. Francescon [36,30], U. Frankenfeld [96], U. Fuchs [36], C. Furget [70], A. Furs [55], M. Fusco Girard [31], J.J. Gaardhøje [79], M. Gagliardi [27], A.M. Gago [102], M. Gallio [27], D.R. Gangadharan [73], P. Ganoti [87], C. Gao [7], C. Garabatos [96], E. Garcia-Solis [13], C. Gargiulo [36], P. Gasik [91], M. Germain [112], A. Gheata [36], M. Gheata [61,36], P. Ghosh [130], S.K. Ghosh [4], P. Gianotti [71], P. Giubellino [36], P. Giubilato [30], E. Gladysz-Dziadus [115], P. Glässel [92], A. Gomez Ramirez [51], P. González-Zamora [10], S. Gorbunov [42], L. Görlich [115], S. Gotovac [114], V. Grabski [63], L.K. Graczykowski [132], A. Grelli [56], A. Grigoras [36], C. Grigoras [36], V. Grigoriev [75], A. Grigoryan [1], S. Grigoryan [65], B. Grinyov [3], N. Grion [109], J.F. Grosse-Oetringhaus [36], J.-Y. Grossiord [128], R. Grosso [36], F. Guber [55], R. Guernane [70], B. Guerzoni [28], K. Gulbrandsen [79], H. Gulkanyan [1], T. Gunji [125], A. Gupta [89], R. Gupta [89], R. Haake [53], Ø. Haaland [18], C. Hadjidakis [50], M. Haiduc [61], H. Hamagaki [125], G. Hamar [134], L.D. Hanratty [101], A. Hansen [79], J.W. Harris [135], H. Hartmann [42], A. Harton [13], D. Hatzifotiadou [104], S. Hayashi [125], S.T. Heckel [52], M. Heide [53], H. Helstrup [37], A. Herghelegiu [77], G. Herrera Corral [11], B.A. Hess [35], K.F. Hetland [37], T.E. Hilden [45], H. Hillemanns [36], B. Hippolyte [54], P. Hristov [36], M. Huang [18], T.J. Humanic [20], N. Hussain [44], T. Hussain [19], D. Hutter [42], D.S. Hwang [21], R. Ilkaev [98], I. Ilkiv [76], M. Inaba [126], C. Ionita [36], M. Ippolitov [75,99], M. Irfan [19], M. Ivanov [96], V. Ivanov [84], V. Izucheev [111], P.M. Jacobs [73], C. Jahnke [118], H.J. Jang [67], M.A. Janik [132], P.H.S.Y. Jayarathna [120], C. Jena [30], S. Jena [120], R.T. Jimenez Bustamante [62], P.G. Jones [101], H. Jung [43], A. Jusko [101], V. Kadyshevskiy [65,i], P. Kalinak [58], A. Kalweit [36], J. Kamin [52], J.H. Kang [136], V. Kaplin [75], S. Kar [130], A. Karasu Uysal [68], O. Karavichev [55], T. Karavicheva [55], E. Karpechev [55], U. Kebschull [51], R. Keidel [137], D.L.D. Keijdener [56], M. Keil [36], K.H. Khan [16], M.M. Khan [19], P. Khan [100], S.A. Khan [130], A. Khanzadeev [84], Y. Kharlov [111], B. Kileng [37], B. Kim [136], D.W. Kim [43,67], D.J. Kim [121], H. Kim [136], J.S. Kim [43], M. Kim [43], M. Kim [136], S. Kim [21], T. Kim [136], S. Kirsch [42], I. Kisel [42], S. Kiselev [57], A. Kisiel [132], G. Kiss [134], J.L. Klay [6], C. Klein [52], J. Klein [92], C. Klein-Bösing [53], A. Kluge [36], M.L. Knichel [92], A.G. Knospe [116], T. Kobayashi [126], C. Kobdaj [113], M. Kofarago [36], M.K. Köhler [96], T. Kollegger [96,42], A. Kolojvari [129], V. Kondratiev [129], N. Kondratyeva [75], E. Kondratyuk [111], A. Konevskikh [55], C. Kouzinopoulos [36], O. Kovalenko [76], V. Kovalenko [129], M. Kowalski [36,115], S. Kox [70], G. Koyithatta Meethaleveedu [47], J. Kral [121], I. Králik [58], A. Kravčáková [40], M. Krelina [39], M. Kretz [42], M. Krivda [58,101], F. Krizek [82], E. Kryshen [36], M. Krzewicki [42,96], A.M. Kubera [20], V. Kučera [82], Y. Kucheriaev [99,i], T. Kugathasan [36], C. Kuhn [54], P.G. Kuijer [80], I. Kulakov [42], J. Kumar [47], L. Kumar [78,86], P. Kurashvili [76], A. Kurepin [55], A.B. Kurepin [55], A. Kuryakin [98], S. Kushpil [82], M.J. Kweon [49], Y. Kwon [136], S.L. La Pointe [110], P. La Rocca [29], C. Lagana Fernandes [118], I. Lakomov [50,36], R. Langoy [41], C. Lara [51], A. Lardeux [15], A. Lattuca [27], E. Laudi [36], R. Lea [26], L. Leardini [92], G.R. Lee [101], S. Lee [136], I. Legrand [36], J. Lehnert [52], R.C. Lemmon [81], V. Lenti [103], E. Leogrande [56], I. León Monzón [117], M. Leoncino [27], P. Lévai [134], S. Li [7,69], X. Li [14], J. Lien [41], R. Lietava [101], S. Lindal [22], V. Lindenstruth [42], C. Lippmann [96], M.A. Lisa [20], H.M. Ljunggren [34], D.F. Lodato [56], P.I. Loenne [18], V.R. Loggins [133], V. Loginov [75], C. Loizides [73], X. Lopez [69], E. López Torres [9], A. Lowe [134], X.-G. Lu [92], P. Luettig [52], M. Lunardon [30], G. Luparello [26,56], A. Maevskaya [55], M. Mager [36], S. Mahajan [89], S.M. Mahmood [22], A. Maire [54], R.D. Majka [135], M. Malaev [84], I. Maldonado Cervantes [62], L. Malinina [65], D. Mal'Kevich [57], P. Malzacher [96], A. Mamonov [98], L. Manceau [110], V. Manko [99], F. Manso [69], V. Manzari [103,36], M. Marchisone [27], J. Mareš [59], G.V. Margagliotti [26], A. Margotti [104], J. Margutti [56], A. Marín [96], C. Markert [116], M. Marquard [52], N.A. Martin [96], J. Martin Blanco [112], P. Martinengo [36], M.I. Martínez [2], G. Martínez García [112], M. Martinez Pedreira [36], Y. Martynov [3], A. Mas [118], S. Masciocchi [96], M. Masera [27], A. Masoni [105], L. Massacrier [112], A. Mastroserio [33], H. Masui [126], A. Matyja [115], C. Mayer [115], J. Mazer [123],

M.A. Mazzoni [108], D. Mcdonald [120], F. Meddi [24], A. Menchaca-Rocha [63], E. Meninno [31], J. Mercado Pérez [92], M. Meres [38], Y. Miake [126], M.M. Mieskolainen [45], K. Mikhaylov [57,65], L. Milano [36], J. Milosevic [22,131], L.M. Minervini [103,23], A. Mischke [56], A.N. Mishra [48], D. Miśkowiec [96], J. Mitra [130], C.M. Mitu [61], N. Mohammadi [56], B. Mohanty [130,78], L. Molnar [54], L. Montaño Zetina [11], E. Montes [10], M. Morando [30], D.A. Moreira De Godoy [112], S. Moretto [30], A. Morreale [112], A. Morsch [36], V. Muccifora [71], E. Mudnic [114], D. Mühlheim [53], S. Muhuri [130], M. Mukherjee [130], H. Müller [36], J.D. Mulligan [135], M.G. Munhoz [118], S. Murray [64], L. Musa [36], J. Musinsky [58], B.K. Nandi [47], R. Nania [104], E. Nappi [103], M.U. Naru [16], C. Nattrass [123], K. Nayak [78], T.K. Nayak [130], S. Nazarenko [98], A. Nedosekin [57], L. Nellen [62], F. Ng [120], M. Nicassio [96], M. Niculescu [61,36], J. Niedziela [36], B.S. Nielsen [79], S. Nikolaev [99], S. Nikulin [99], V. Nikulin [84], F. Noferini [12,104], P. Nomokonov [65], G. Nooren [56], J. Norman [122], A. Nyanin [99], J. Nystrand [18], H. Oeschler [92], S. Oh [135], S.K. Oh [66], A. Ohlson [36], A. Okatan [68], T. Okubo [46], L. Olah [134], J. Oleniacz [132], A.C. Oliveira Da Silva [118], M.H. Oliver [135], J. Onderwaater [96], C. Oppedisano [110], A. Ortiz Velasquez [62], A. Oskarsson [34], J. Otwinowski [96,115], K. Oyama [92], M. Ozdemir [52], Y. Pachmayer [92], P. Pagano [31], G. Paić [62], C. Pajares [17], S.K. Pal [130], J. Pan [133], D. Pant [47], V. Papikyan [1], G.S. Pappalardo [106], P. Pareek [48], W.J. Park [96], S. Parmar [86], A. Passfeld [53], V. Paticchio [103], B. Paul [100], T. Pawlak [132], T. Peitzmann [56], H. Pereira Da Costa [15], E. Pereira De Oliveira Filho [118], D. Peresunko [75,99], C.E. Pérez Lara [80], V. Peskov [52], Y. Pestov [5], V. Petráček [39], V. Petrov [111], M. Petrovici [77], C. Petta [29], S. Piano [109], M. Pikna [38], P. Pillot [112], O. Pinazza [104,36], L. Pinsky [120], D.B. Piyarathna [120], M. Płoskoń [73], M. Planinic [127], J. Pluta [132], S. Pochybova [134], P.L.M. Podesta-Lerma [117], M.G. Poghosyan [85], B. Polichtchouk [111], N. Poljak [127], W. Poonsawat [113], A. Pop [77], S. Porteboeuf-Houssais [69], J. Porter [73], J. Pospisil [82], S.K. Prasad [4], R. Preghenella [104,36], F. Prino [110], C.A. Pruneau [133], I. Pshenichnov [55], M. Puccio [110], G. Puddu [25], P. Pujahari [133], V. Punin [98], J. Putschke [133], H. Qvigstad [22], A. Rachevski [109], S. Raha [4], S. Rajput [89], J. Rak [121], A. Rakotozafindrabe [15], L. Ramello [32], R. Raniwala [90], S. Raniwala [90], S.S. Räsänen [45], B.T. Rascanu [52], D. Rathee [86], K.F. Read [123], J.S. Real [70], K. Redlich [76], R.J. Reed [133], A. Rehman [18], P. Reichelt [52], M. Reicher [56], F. Reidt [36,92], X. Ren [7], R. Renfordt [52], A.R. Reolon [71], A. Reshetin [55], F. Rettig [42], J.-P. Revol [12], K. Reygers [92], V. Riabov [84], R.A. Ricci [72], T. Richert [34], M. Richter [22], P. Riedler [36], W. Riegler [36], F. Riggi [29], C. Ristea [61], A. Rivetti [110], E. Rocco [56], M. Rodríguez Cahuantzi [2,11], A. Rodriguez Manso [80], K. Røed [22], E. Rogochaya [65], D. Rohr [42], D. Röhrich [18], R. Romita [122], F. Ronchetti [71], L. Ronflette [112], P. Rosnet [69], A. Rossi [36], F. Roukoutakis [87], A. Roy [48], C. Roy [54], P. Roy [100], A.J. Rubio Montero [10], R. Rui [26], R. Russo [27], E. Ryabinkin [99], Y. Ryabov [84], A. Rybicki [115], S. Sadovsky [111], K. Šafařík [36], B. Sahlmuller [52], P. Sahoo [48], R. Sahoo [48], S. Sahoo [60], P.K. Sahu [60], J. Saini [130], S. Sakai [71], M.A. Saleh [133], C.A. Salgado [17], J. Salzwedel [20], S. Sambyal [89], V. Samsonov [84], X. Sanchez Castro [54], L. Šándor [58], A. Sandoval [63], M. Sano [126], G. Santagati [29], D. Sarkar [130], E. Scapparone [104], F. Scarlassara [30], R.P. Scharenberg [94], C. Schiaua [77], R. Schicker [92], C. Schmidt [96], H.R. Schmidt [35], S. Schuchmann [52], J. Schukraft [36], M. Schulc [39], T. Schuster [135], Y. Schutz [112,36], K. Schwarz [96], K. Schweda [96], G. Scioli [28], E. Scomparin [110], R. Scott [123], K.S. Seeder [118], J.E. Seger [85], Y. Sekiguchi [125], I. Selyuzhenkov [96], K. Senosi [64], J. Seo [66,95], E. Serradilla [10,63], A. Sevcenco [61], A. Shabanov [55], A. Shabetai [112], O. Shadura [3], R. Shahoyan [36], A. Shangaraev [111], A. Sharma [89], N. Sharma [60,123], K. Shigaki [46], K. Shtejer [9,27], Y. Sibiriak [99], S. Siddhanta [105], K.M. Sielewicz [36], T. Siemiarczuk [76], D. Silvermyr [83,34], C. Silvestre [70], G. Simatovic [127], G. Simonetti [36], R. Singaraju [130], R. Singh [78], S. Singha [78,130], V. Singhal [130], B.C. Sinha [130], T. Sinha [100], B. Sitar [38], M. Sitta [32], T.B. Skaali [22], M. Slupecki [121], N. Smirnov [135], R.J.M. Snellings [56], T.W. Snellman [121], C. Søgaard [34], R. Soltz [74], J. Song [95], M. Song [136], Z. Song [7], F. Soramel [30], S. Sorensen [123], M. Spacek [39], E. Spiriti [71], I. Sputowska [115], M. Spyropoulou-Stassinaki [87], B.K. Srivastava [94], J. Stachel [92], I. Stan [61], G. Stefanek [76], M. Steinpreis [20], E. Stenlund [34], G. Steyn [64], J.H. Stiller [92], D. Stocco [112], P. Strmen [38], A.A.P. Suaide [118], T. Sugitate [46], C. Suire [50], M. Suleymanov [16], R. Sultanov [57], M. Šumbera [82], T.J.M. Symons [73], A. Szabo [38], A. Szanto de Toledo [118], I. Szarka [38], A. Szczepankiewicz [36], M. Szymanski [132], J. Takahashi [119], N. Tanaka [126], M.A. Tangaro [33], J.D. Tapia Takaki [50], A. Tarantola Peloni [52], M. Tariq [19], M.G. Tarzila [77], A. Tauro [36], G. Tejeda Muñoz [2], A. Telesca [36], K. Terasaki [125], C. Terrevoli [30,25], B. Teyssier [128], J. Thäder [96,73], D. Thomas [116], R. Tieulent [128], A.R. Timmins [120], A. Toia [52], S. Trogolo [110], V. Trubnikov [3], W.H. Trzaska [121], T. Tsuji [125], A. Tumkin [98], R. Turrisi [107], T.S. Tveter [22], K. Ullaland [18], A. Uras [128], G.L. Usai [25], A. Utrobicic [127], M. Vajzer [82], M. Vala [58], L. Valencia Palomo [69], S. Vallero [27], J. Van Der Maarel [56], J.W. Van Hoorne [36],

M. van Leeuwen [56], T. Vanat [82], P. Vande Vyvre [36], D. Varga [134], A. Vargas [2], M. Vargyas [121], R. Varma [47], M. Vasileiou [87], A. Vasiliev [99], A. Vauthier [70], V. Vechernin [129], A.M. Veen [56], M. Veldhoen [56], A. Velure [18], M. Venaruzzo [72], E. Vercellin [27], S. Vergara Limón [2], R. Vernet [8], M. Verweij [133], L. Vickovic [114], G. Viesti [30,i], J. Viinikainen [121], Z. Vilakazi [124], O. Villalobos Baillie [101], A. Vinogradov [99], L. Vinogradov [129], Y. Vinogradov [98], T. Virgili [31], V. Vislavicius [34], Y.P. Viyogi [130], A. Vodopyanov [65], M.A. Völkl [92], K. Voloshin [57], S.A. Voloshin [133], G. Volpe [36,134], B. von Haller [36], I. Vorobyev [91], D. Vranic [96,36], J. Vrláková [40], B. Vulpescu [69], A. Vyushin [98], B. Wagner [18], J. Wagner [96], H. Wang [56], M. Wang [7,112], Y. Wang [92], D. Watanabe [126], M. Weber [36,120], S.G. Weber [96], J.P. Wessels [53], U. Westerhoff [53], J. Wiechula [35], J. Wikne [22], M. Wilde [53], G. Wilk [76], J. Wilkinson [92], M.C.S. Williams [104], B. Windelband [92], M. Winn [92], C.G. Yaldo [133], Y. Yamaguchi [125], H. Yang [56], P. Yang [7], S. Yano [46], S. Yasnopolskiy [99], Z. Yin [7], H. Yokoyama [126], I.-K. Yoo [95], V. Yurchenko [3], I. Yushmanov [99], A. Zaborowska [132], V. Zaccolo [79], A. Zaman [16], C. Zampolli [104], H.J.C. Zanoli [118], S. Zaporozhets [65], A. Zarochentsev [129], P. Závada [59], N. Zaviyalov [98], H. Zbroszczyk [132], I.S. Zgura [61], M. Zhalov [84], H. Zhang [7], X. Zhang [73], Y. Zhang [7], C. Zhao [22], N. Zhigareva [57], D. Zhou [7], Y. Zhou [56], Z. Zhou [18], H. Zhu [7], J. Zhu [7,112], X. Zhu [7], A. Zichichi [12,28], A. Zimmermann [92], M.B. Zimmermann [53,36], G. Zinovjev [3], M. Zyzak [42]

[1] *A.I. Alikhanyan National Science Laboratory (Yerevan Physics Institute) Foundation, Yerevan, Armenia*
[2] *Benemérita Universidad Autónoma de Puebla, Puebla, Mexico*
[3] *Bogolyubov Institute for Theoretical Physics, Kiev, Ukraine*
[4] *Bose Institute, Department of Physics and Centre for Astroparticle Physics and Space Science (CAPSS), Kolkata, India*
[5] *Budker Institute for Nuclear Physics, Novosibirsk, Russia*
[6] *California Polytechnic State University, San Luis Obispo, CA, United States*
[7] *Central China Normal University, Wuhan, China*
[8] *Centre de Calcul de l'IN2P3, Villeurbanne, France*
[9] *Centro de Aplicaciones Tecnológicas y Desarrollo Nuclear (CEADEN), Havana, Cuba*
[10] *Centro de Investigaciones Energéticas Medioambientales y Tecnológicas (CIEMAT), Madrid, Spain*
[11] *Centro de Investigación y de Estudios Avanzados (CINVESTAV), Mexico City and Mérida, Mexico*
[12] *Centro Fermi – Museo Storico della Fisica e Centro Studi e Ricerche "Enrico Fermi", Rome, Italy*
[13] *Chicago State University, Chicago, IL, USA*
[14] *China Institute of Atomic Energy, Beijing, China*
[15] *Commissariat à l'Energie Atomique, IRFU, Saclay, France*
[16] *COMSATS Institute of Information Technology (CIIT), Islamabad, Pakistan*
[17] *Departamento de Física de Partículas and IGFAE, Universidad de Santiago de Compostela, Santiago de Compostela, Spain*
[18] *Department of Physics and Technology, University of Bergen, Bergen, Norway*
[19] *Department of Physics, Aligarh Muslim University, Aligarh, India*
[20] *Department of Physics, Ohio State University, Columbus, OH, United States*
[21] *Department of Physics, Sejong University, Seoul, South Korea*
[22] *Department of Physics, University of Oslo, Oslo, Norway*
[23] *Dipartimento di Elettrotecnica ed Elettronica del Politecnico, Bari, Italy*
[24] *Dipartimento di Fisica dell'Università 'La Sapienza' and Sezione INFN Rome, Italy*
[25] *Dipartimento di Fisica dell'Università and Sezione INFN, Cagliari, Italy*
[26] *Dipartimento di Fisica dell'Università and Sezione INFN, Trieste, Italy*
[27] *Dipartimento di Fisica dell'Università and Sezione INFN, Turin, Italy*
[28] *Dipartimento di Fisica e Astronomia dell'Università and Sezione INFN, Bologna, Italy*
[29] *Dipartimento di Fisica e Astronomia dell'Università and Sezione INFN, Catania, Italy*
[30] *Dipartimento di Fisica e Astronomia dell'Università and Sezione INFN, Padova, Italy*
[31] *Dipartimento di Fisica 'E.R. Caianiello' dell'Università and Gruppo Collegato INFN, Salerno, Italy*
[32] *Dipartimento di Scienze e Innovazione Tecnologica dell'Università del Piemonte Orientale and Gruppo Collegato INFN, Alessandria, Italy*
[33] *Dipartimento Interateneo di Fisica 'M. Merlin' and Sezione INFN, Bari, Italy*
[34] *Division of Experimental High Energy Physics, University of Lund, Lund, Sweden*
[35] *Eberhard Karls Universität Tübingen, Tübingen, Germany*
[36] *European Organization for Nuclear Research (CERN), Geneva, Switzerland*
[37] *Faculty of Engineering, Bergen University College, Bergen, Norway*
[38] *Faculty of Mathematics, Physics and Informatics, Comenius University, Bratislava, Slovakia*
[39] *Faculty of Nuclear Sciences and Physical Engineering, Czech Technical University in Prague, Prague, Czech Republic*
[40] *Faculty of Science, P.J. Šafárik University, Košice, Slovakia*
[41] *Faculty of Technology, Buskerud and Vestfold University College, Vestfold, Norway*
[42] *Frankfurt Institute for Advanced Studies, Johann Wolfgang Goethe-Universität Frankfurt, Frankfurt, Germany*
[43] *Gangneung-Wonju National University, Gangneung, South Korea*
[44] *Gauhati University, Department of Physics, Guwahati, India*
[45] *Helsinki Institute of Physics (HIP), Helsinki, Finland*
[46] *Hiroshima University, Hiroshima, Japan*
[47] *Indian Institute of Technology Bombay (IIT), Mumbai, India*
[48] *Indian Institute of Technology Indore, Indore (IITI), India*
[49] *Inha University, Incheon, South Korea*
[50] *Institut de Physique Nucléaire d'Orsay (IPNO), Université Paris-Sud, CNRS–IN2P3, Orsay, France*
[51] *Institut für Informatik, Johann Wolfgang Goethe-Universität Frankfurt, Frankfurt, Germany*
[52] *Institut für Kernphysik, Johann Wolfgang Goethe-Universität Frankfurt, Frankfurt, Germany*
[53] *Institut für Kernphysik, Westfälische Wilhelms-Universität Münster, Münster, Germany*
[54] *Institut Pluridisciplinaire Hubert Curien (IPHC), Université de Strasbourg, CNRS–IN2P3, Strasbourg, France*
[55] *Institute for Nuclear Research, Academy of Sciences, Moscow, Russia*
[56] *Institute for Subatomic Physics of Utrecht University, Utrecht, Netherlands*

[57] *Institute for Theoretical and Experimental Physics, Moscow, Russia*
[58] *Institute of Experimental Physics, Slovak Academy of Sciences, Košice, Slovakia*
[59] *Institute of Physics, Academy of Sciences of the Czech Republic, Prague, Czech Republic*
[60] *Institute of Physics, Bhubaneswar, India*
[61] *Institute of Space Science (ISS), Bucharest, Romania*
[62] *Instituto de Ciencias Nucleares, Universidad Nacional Autónoma de México, Mexico City, Mexico*
[63] *Instituto de Física, Universidad Nacional Autónoma de México, Mexico City, Mexico*
[64] *iThemba LABS, National Research Foundation, Somerset West, South Africa*
[65] *Joint Institute for Nuclear Research (JINR), Dubna, Russia*
[66] *Konkuk University, Seoul, South Korea*
[67] *Korea Institute of Science and Technology Information, Daejeon, South Korea*
[68] *KTO Karatay University, Konya, Turkey*
[69] *Laboratoire de Physique Corpusculaire (LPC), Clermont Université, Université Blaise Pascal, CNRS–IN2P3, Clermont-Ferrand, France*
[70] *Laboratoire de Physique Subatomique et de Cosmologie, Université Grenoble-Alpes, CNRS–IN2P3, Grenoble, France*
[71] *Laboratori Nazionali di Frascati, INFN, Frascati, Italy*
[72] *Laboratori Nazionali di Legnaro, INFN, Legnaro, Italy*
[73] *Lawrence Berkeley National Laboratory, Berkeley, CA, United States*
[74] *Lawrence Livermore National Laboratory, Livermore, CA, United States*
[75] *Moscow Engineering Physics Institute, Moscow, Russia*
[76] *National Centre for Nuclear Studies, Warsaw, Poland*
[77] *National Institute for Physics and Nuclear Engineering, Bucharest, Romania*
[78] *National Institute of Science Education and Research, Bhubaneswar, India*
[79] *Niels Bohr Institute, University of Copenhagen, Copenhagen, Denmark*
[80] *Nikhef, National Institute for Subatomic Physics, Amsterdam, Netherlands*
[81] *Nuclear Physics Group, STFC Daresbury Laboratory, Daresbury, United Kingdom*
[82] *Nuclear Physics Institute, Academy of Sciences of the Czech Republic, Řež u Prahy, Czech Republic*
[83] *Oak Ridge National Laboratory, Oak Ridge, TN, United States*
[84] *Petersburg Nuclear Physics Institute, Gatchina, Russia*
[85] *Physics Department, Creighton University, Omaha, NE, United States*
[86] *Physics Department, Panjab University, Chandigarh, India*
[87] *Physics Department, University of Athens, Athens, Greece*
[88] *Physics Department, University of Cape Town, Cape Town, South Africa*
[89] *Physics Department, University of Jammu, Jammu, India*
[90] *Physics Department, University of Rajasthan, Jaipur, India*
[91] *Physik Department, Technische Universität München, Munich, Germany*
[92] *Physikalisches Institut, Ruprecht-Karls-Universität Heidelberg, Heidelberg, Germany*
[93] *Politecnico di Torino, Turin, Italy*
[94] *Purdue University, West Lafayette, IN, United States*
[95] *Pusan National University, Pusan, South Korea*
[96] *Research Division and ExtreMe Matter Institute EMMI, GSI Helmholtzzentrum für Schwerionenforschung, Darmstadt, Germany*
[97] *Rudjer Bošković Institute, Zagreb, Croatia*
[98] *Russian Federal Nuclear Center (VNIIEF), Sarov, Russia*
[99] *Russian Research Centre Kurchatov Institute, Moscow, Russia*
[100] *Saha Institute of Nuclear Physics, Kolkata, India*
[101] *School of Physics and Astronomy, University of Birmingham, Birmingham, United Kingdom*
[102] *Sección Física, Departamento de Ciencias, Pontificia Universidad Católica del Perú, Lima, Peru*
[103] *Sezione INFN, Bari, Italy*
[104] *Sezione INFN, Bologna, Italy*
[105] *Sezione INFN, Cagliari, Italy*
[106] *Sezione INFN, Catania, Italy*
[107] *Sezione INFN, Padova, Italy*
[108] *Sezione INFN, Rome, Italy*
[109] *Sezione INFN, Trieste, Italy*
[110] *Sezione INFN, Turin, Italy*
[111] *SSC IHEP of NRC Kurchatov institute, Protvino, Russia*
[112] *SUBATECH, Ecole des Mines de Nantes, Université de Nantes, CNRS–IN2P3, Nantes, France*
[113] *Suranaree University of Technology, Nakhon Ratchasima, Thailand*
[114] *Technical University of Split FESB, Split, Croatia*
[115] *The Henryk Niewodniczanski Institute of Nuclear Physics, Polish Academy of Sciences, Cracow, Poland*
[116] *The University of Texas at Austin, Physics Department, Austin, TX, USA*
[117] *Universidad Autónoma de Sinaloa, Culiacán, Mexico*
[118] *Universidade de São Paulo (USP), São Paulo, Brazil*
[119] *Universidade Estadual de Campinas (UNICAMP), Campinas, Brazil*
[120] *University of Houston, Houston, TX, United States*
[121] *University of Jyväskylä, Jyväskylä, Finland*
[122] *University of Liverpool, Liverpool, United Kingdom*
[123] *University of Tennessee, Knoxville, TN, United States*
[124] *University of the Witwatersrand, Johannesburg, South Africa*
[125] *University of Tokyo, Tokyo, Japan*
[126] *University of Tsukuba, Tsukuba, Japan*
[127] *University of Zagreb, Zagreb, Croatia*
[128] *Université de Lyon, Université Lyon 1, CNRS/IN2P3, IPN-Lyon, Villeurbanne, France*
[129] *V. Fock Institute for Physics, St. Petersburg State University, St. Petersburg, Russia*
[130] *Variable Energy Cyclotron Centre, Kolkata, India*
[131] *Vinča Institute of Nuclear Sciences, Belgrade, Serbia*
[132] *Warsaw University of Technology, Warsaw, Poland*
[133] *Wayne State University, Detroit, MI, United States*
[134] *Wigner Research Centre for Physics, Hungarian Academy of Sciences, Budapest, Hungary*
[135] *Yale University, New Haven, CT, United States*

[136] *Yonsei University, Seoul, South Korea*
[137] *Zentrum für Technologietransfer und Telekommunikation (ZTT), Fachhochschule Worms, Worms, Germany*

[i] Deceased.